JAKU: Earth Sci., **Vol. 24,** No. 1, pp: 1-17 (2013 A.D. / 1434 A.H.)
DOI: 10.4197 / Ear. 24-1.1

Potential Field Methods to Investigate the Source of Hydrocarbon Contamination in Sharm El-Maya Bay Area, Sharm El-Sheikh, Egypt

M.A. Morsy, M.A. Rashed[*], N.N. El-Masry[*], F.A. Soliman
Geology Department, Suez Canal University, Ismailia, Egypt
[*] *Faculty of Earth Sciences, King Abdulaziz University, Saudi Arabia*
Email address: rashedmohamed@gmail.com

Received: 16/10/2011 Accepted: 7/5/2012

Abstract. Hydrocarbon contamination in Sharm El-Maya Bay forms an eminent threat to the flourishing tourism industry in Sharm El-Sheikh area. Chemical analyses of seawater, seabed sediments and surface soil samples indicate anomalously high level of hydrocarbon contamination in Sharm El-Maya Bay area. Integrated geophysical survey using magnetic and gravity methods was conducted on the suspected area in order to delineate the source(s) of contamination. The magnetic survey results revealed the presence of four possible sites of subsurface storage facilities. Three of them have been confirmed by the gravity survey results. Moreover, the gravity survey revealed the presence of north-south trending fault on the eastern side of the study area. Detailed investigations using high-resolution geophysical tool, such as ground penetrating radar, are needed to get better imaging of the vertical and horizontal distribution of the subsurface objects in the study area before the excavation.

Keywords: Gravity, Magnetic, Contamination, Tank, Pipe, Sinai.

Introduction

During the past two decades, Sharm El-Sheikh area has evolved into an international resort visited by millions of tourists from all over the world every year. The main reason of attraction of Sharm El-Sheikh area is its virgin nature and hygienic beaches. Sharm El-Maya Bay is a small semicircular bay located in the southern suburb of Sharm El-Sheikh City

(Fig. 1). In 1999, the bay was devastated by the spilling of huge amounts of oil into its waters. These unfortunate oil spills in Sharm El-Maya Bay formed a direct threat to the blooming tourism industry in the entire area.

Fig. 1. Location map of Sharm El-Maya Bay area and its surroundings.

Although, immediate remedy procedures were applied to contain the spilling and mitigate the damage, the source of the spill is still a controversial issue till today. Some think that the spill was caused by the inappropriate dismantling of the old power plant and its surface fuel storage tanks (Suez Canal University Report, 1999; Cairo University Report, 2001). This power plant was located on the shoe-shaped headland defining the southwestern border of the bay and was dismantled few months before the spilling incident (Fig. 1). Others, however, suggested that oil contamination could be ascribed to spilled crude oil, dumped oil wastes, and leaked fuel from boats (Khattab *et al.*, 2006). Some concluded that the source of oil polluting the waters of the bay is buried within the subsurface of the southwestern headland and that the area is still under great threat from a persistent source of oil contamination (Morsy *et al.*, 2010).

The southwestern headland forms a shoe-shaped promontory projecting into the Red Sea and separates Sharm El-Maya Bay from the neighboring Sharm El-Sheikh Bay. The bay is located very close to the

intersection of the Aqaba–Dead Sea rift with the Gulf of Suez and the Red Sea rifts (Fig. 1). The study area covers the northwestern corner of the headland on the periphery of Sharm El-Maya Bay and its mouth to the Red Sea. The study was focused on this part of the headland because of the high concentration of surface contamination and because of accessibility.

The headland forms an elevated tract of near-flat-land surface bounded seaward by prominent sea cliffs, which border the southern margin of the bay as well as the waterway to its mouth (Fig. 1). The sea cliffs around the headland are distinguished into steeply sloping cliffs, composed of alternating beds of clastic sedimentary rocks and coralline limestone, and crumbling slopes, composed of unconsolidated sediments and slumped blocks of clastic sedimentary rocks and coralline limestone.

Chemical analyses conducted on samples collected from the headland soil, seabed sediments and bay water showed high level of hydrocarbon contamination in all samples. The analysis results showed that the average concentration of the total hydrocarbons was 661.7±383.16 μg/g in the headland soil, 170±128.59 μg/g in the seabed, and 37.99±17.45 mg/L in the seawater (Morsy *et al.,* 2010). The results also suggested a land-based source of pollution.

Gravity and Magnetic methods were proved successful in detecting and delineating underground cavities and foreign objects buried in different environments (Allred *et al.*, 2004; Debeglia and Dupont, 2002; Gilkeson *et al.*, 1986; Hinze, 1990 andMochales *et al.*, 2008). The magnetic method gives a well-distinguished response to buried artificial objects with different magnetic properties from the surrounding material, while gravity method precisely maps the variation in subsurface densities. A combination of both methods can be very successful in distinguishing buried source(s) of contamination such as underground hydrocarbon storage facilities. Accordingly, an integrated gravity and magnetic survey was conducted in the study area to delineate possible source(s) of hydrocarbon contamination buried under the southwestern headland of Sharm El-Maya Bay area.

Magnetic Survey

The goal of magnetic survey in an area is to investigate the subsurface on the basis of the variations in the Earth's magnetic field

resulting from the magnetic properties of subsurface material. Many examples of successfully detecting buried ferromagnetic objects by magnetic survey are cited in the literatures (Furness, 2002; Horton *et al.*, 1993, Horton, 2003, Marchetti *et al.*, 2002 and Missiaen and Feller, 2008).

In Sharm El-Maya area, the magnetic survey was planned to cover the study area with enough measurements to detect and delineate any subsurface, natural or artificial, magnetically anomalous objects. A SCINTREX Fluxgate magnetometer (MFD-4) was used to collect field data. Vertical magnetic field strength was measured over 139 field stations (Fig. 2). At every station, measurements were conducted at two sensor heights, which are 45 and 90 cm above the ground surface. A base station was established in the central part of the study area and was regularly revisited during data collection. Base station measurements were later used to correct the magnetic survey data for diurnal variations in the Earth's magnetic field. Station interval and profile separation varied between 5 and 25 meters based on ground surface conditions. Field station locations were selected to cover most of the suspected sites, particularly those stained with oily spots.

Fig. 2. A map showing the locations of magnetic field stations (black dotes) and the base station (white star) in the study area.

Horizontal and vertical controls of the field stations were conducted using a couple of Garmin's GPSMAP® 60cs receivers. One GPS

receiver was left over at the base station position to record satellite data every one second and store it on an attached portable computer. While the other GPS receiver was moving with the magnetometer operator. Data from both GPS devices were subjected to differential processing to correct any changes in GPS data that could be caused by errors in the satellite path. The differential processing resulted in position solutions with a standard deviation less than one meter in X, Y, and Z directions. The corrected GPS data were then used to set the positioning of the field stations.

The study area is almost a perfect flat-topped tract of land with negligible latitude variations. Therefore, no elevation correction was needed for the collected data. Latitude correction was not also required because the study area is relatively small. However, magnetic field measurements were corrected for diurnal variations because they were collected over a long span of time. The drift correction was conducted using the base station readings assuming linear interpolation between successive base station readings. The corrected vertical magnetic field strength readings at sensor heights 45 and 90 cm above the ground surface as well as the vertical magnetic gradient data were then presented as contour maps using Surfer® 8.0 provided by Golden Software Inc., 2002 (Fig. 3, 4, and 5).

Interpretation of magnetic anomalies is a complex process because of the several factors involved in shaping a magnetic anomaly such as the magnetic susceptibility of the causing subsurface body and the strength and orientation of the Earth's magnetic field at the survey location (Dobrin and Savit, 1988). However, five anomalies can be confidently recognized in all magnetic maps (Fig. 3, 4, and 5). The first anomaly is located in the western part of the study area and shows as two sets of elliptical-shaped concentric contour lines. The long axis of the anomaly trends northwest–southeast and is about 28 meters, whereas the short axis trends east-northeast–west-southwest and is about 18 meters.

The second anomaly lies to the east of the first anomaly and is also depicted in all magnetic maps (Fig. 3, 4, and 5). The center of this anomaly lies at about 40 meters to the east of the center of anomaly number (1). The resemblance between the 2 anomalies may indicate that theymay be caused by two subsurface objects similar in dimensions and

is buried at approximately the same depth. The depth to the top of the buried body, as calculated from the magnetic anomaly, is 3.3 meters.

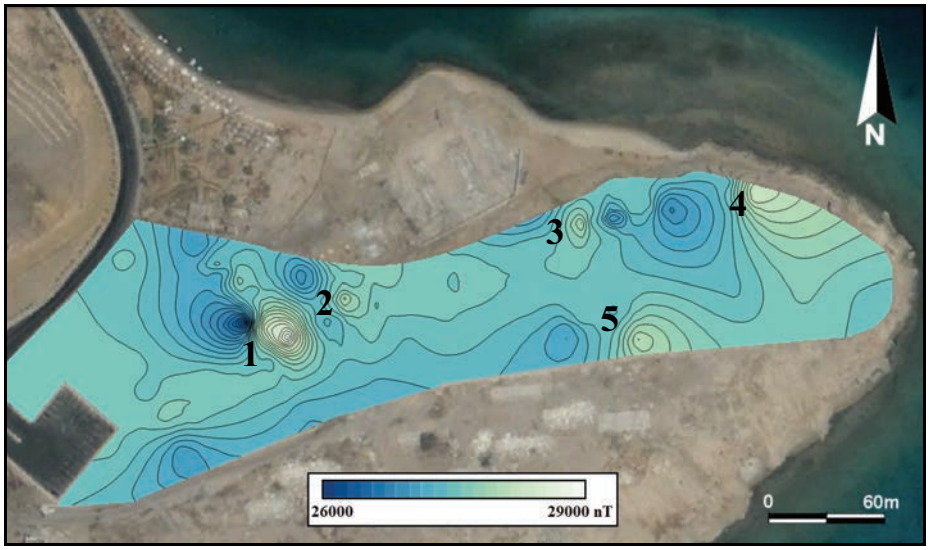

Fig. 3. Vertical magnetic field strength contour map of the study area (Sensor height: 90cm and contour interval: 200 nT).

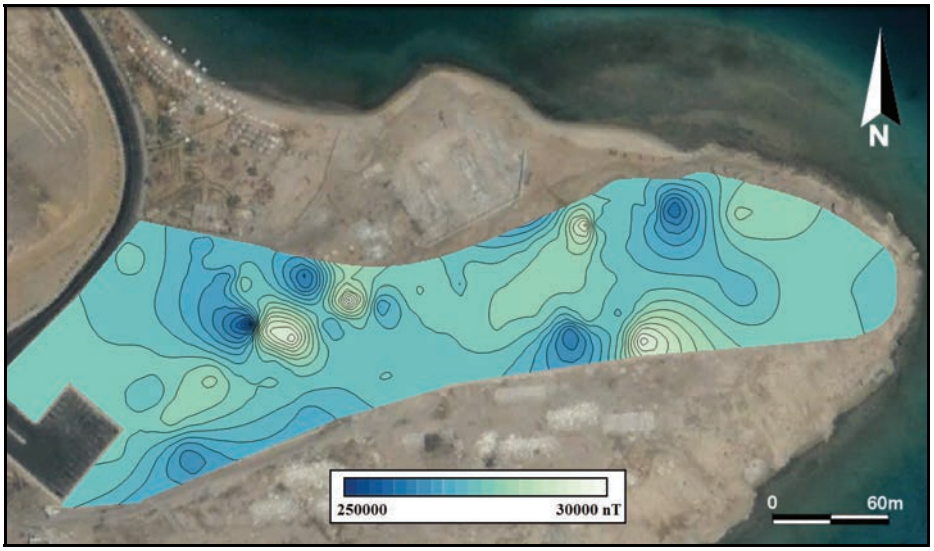

Fig. 4. Vertical magnetic field strength contour map of the study area (Sensor height: 45cm and contour interval: 200 nT).

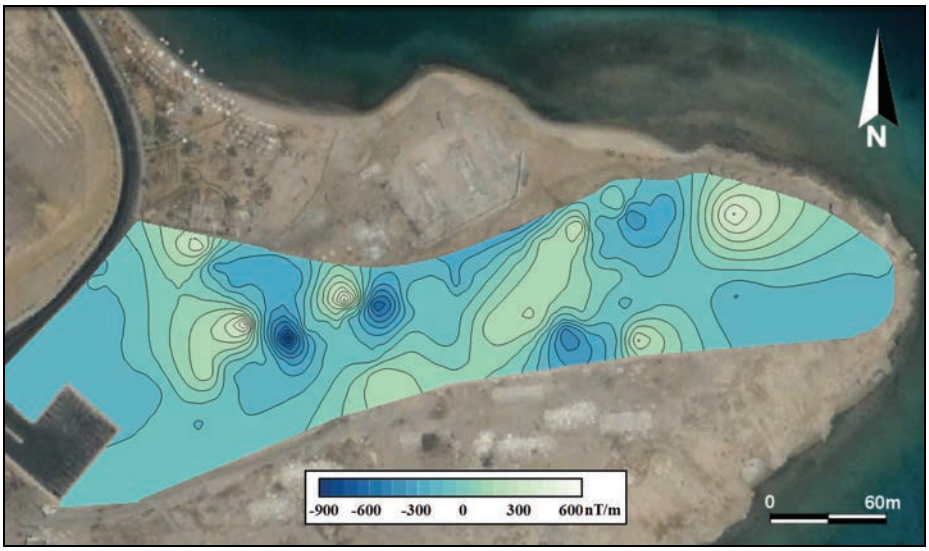

Fig. 5. Vertical magnetic gradient contour map of the study area (Contour interval: 100nT/m).

The third anomaly lies about 140 meters to the northeast of the second anomaly and is aligned with the first and the second anomalies on a north northeast-south southwest trend. The average depth to the buried body, as estimated from magnetic maps, is about 4.2 meters.

The fourth anomaly lies at about 270 meters to the northeast of the center of the first anomaly and is aligned with the previously depicted anomalies. From the shape of the magnetic gradient anomaly. This subsurface body may have the same dimensions of the unearthed bodies depicted from previous anomalies. The depth to this body is 5.6 meters.

The shape and character of the abovementioned anomalies, as well as the observed surface structures in the field, may indicate that they are caused by either empty or filled reinforced-concrete tanks.

The fifth anomaly is a strong anomaly that can be easily recognized on the 45 and 90 cm-height vertical magnetic field strength contour maps (Fig. 3, 4, and 5). It lies at about 75 meters to the south of the fourth anomaly and shows two sets of concentric contour lines separated by evenly spaced parallel contour lines. This anomaly is considered, however, as insignificant, because it was mainly caused by a surface reinforced-concrete foundation left behind after dismantling the electric power plant (Fig. 2).

In this study, field magnetic survey was used to investigate the presence of buried objects of different magnetic properties than their surroundings. In general, the magnetic survey was successful in delineating four areas of interest where similar reinforced concrete tanks may be present in the underground. The quality of the magnetic survey data, however, were highly affected by the presence of surface reinforced concrete structures that are widespread in the study area and represent a major source of noise. The fifth anomaly is a good example of such a surface noise. Moreover, the survey revealed a number of suspicious anomalies next to the wall, which delimits the southern border of the study area. These anomalies may represent significant subsurface structures of yet unknown nature that could be related to the pollution afflicting the study area. Therefore, it was necessary to conduct further geophysical studies using a different surveying technique that is less affected by surface sources of noise to confirm and define the nature of the buried subsurface structures in the study area.

Gravity Survey

A gravity survey investigates the differences in the Earth's gravitational field within an area. These differences in the gravitational field are attributed to differences in subsurface densities. In recent decades, gravity survey has been widely used to tackle different environmental and engineering problems such as detecting buried cavities, tanks, infrastructures, and landfills (Butler, 1984; Butler, 2001; Hare *et al.*, 1999; Roberts *et al.*, 1990; Rybakov *et al.*, 2001 and Yule *et al.*, 1998). In this study, gravity measurements were collected over 107 field stations, with station spacing varying between 5 and 15 meters, to further investigate the interesting sites revealed by the magnetic survey (Fig. 6).

Gravity data were collected using a Worden gravimeter manufactured by Houston Technical Laboratories (HTL). A base station was established in the central part of the study area and was revisited approximately every one hour. Data collected over the base station were used later to correct gravity survey data for temporal variations in the Earth's gravitational field. Horizontal and vertical controls of field stations were conducted using the same procedure described earlier during the magnetic survey.

Fig. 6. A map showing the locations of gravity field stations (black dots) and the base station (white star) in the study area.

As mentioned earlier, the study area is almost a perfect small flat-topped tract of land with almost no altitude variations; hence, no latitude, free air, Bouguer, and terrain corrections were needed for the collected data. However, the collected gravitational acceleration field measurements were corrected for temporal variations, such as instrumental drift and tidal effects. After data correction, the resultant Bouguer gravity data,should correlate only with lateral variations in the density of the upper crust. These were obtained by subtracting all the corrected gravity data from a definite base station value (Reynolds, 1997) and representing them on a contour map (Fig. 7).

The western and the central parts of the Bouguer anomaly map are characterized by widely spaced sub-parallel contour lines, which are superimposed by small concentric contour lines at some sites (Fig. 7). The eastern part of the map, however, is characterized by very closely spaced parallel contour lines, trending north-south. It is obvious that the Bouguer anomaly map is a combination of short wavelength anomalies superimposed on a long wavelength anomaly. The short wavelength, or residual, anomalies are resulted from small shallow objects buried in the study area, whereas the long wavelength, or regional, anomaly is related to a large-scale geological structure, which dominates the area and greatly masks the short wavelength anomalies.

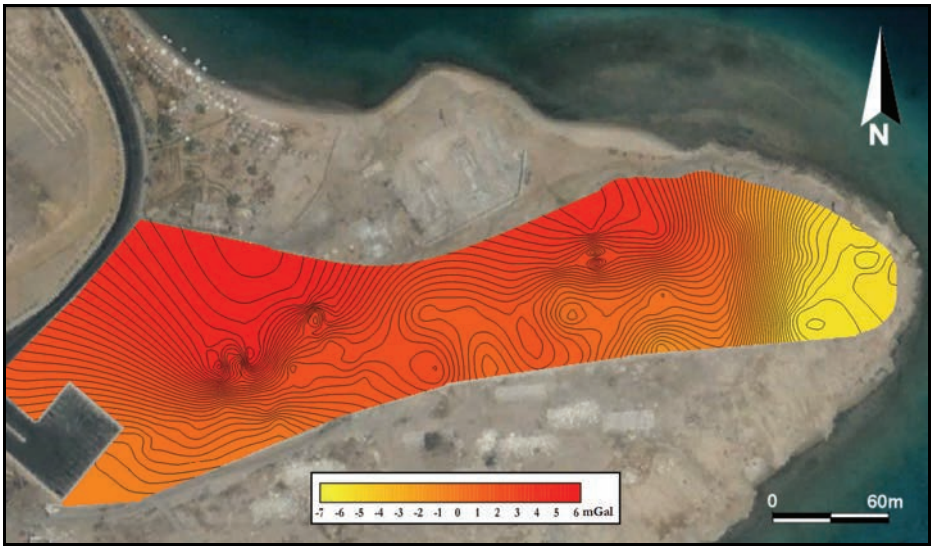

Fig. 7. Bouguer anomaly map of the study area (Contour interval: 0.2mGal).

There are various techniques to obtain the regional gravity anomaly and the residual gravity anomalies from a Bouguer gravity map. Some of these techniques are graphical and others are analytical. Commonly used analytical techniques include surface fitting, frequency filtering, and downward continuation (NJDEP, 2005). A computer-based filtering method was applied to the collected data to isolate regional and residual anomalies (Fig. 8 and 9). The filtering algorithm calculates the difference between the real value of a point in a grid and the hypothetical value of the same point as calculated from the interpolation of the surrounding points. This is the same principle of Griffin (1949) method that can be summarized in the following equation:

$$g_{regional} = (g_1 + g_2 + \ldots + g_n)/n$$

Where ($g_{regional}$) is the regional gravity of a point, and ($g_1+g_2+\ldots+g_n$) are the (g) values of a number of points surrounding this point, and (n) is the number of these points. The residual gravity can be then calculated by subtracting the regional gravity value from the Bouguer gravity value.

The gravity survey did not only confirm the results of the magnetic survey, but also unexpectedly revealed the existence of a large-scale geological structure dominating the study area. The gravity survey also indicated the presence of small-scale subsurface artificial structures, which were unnoticed during the magnetic survey.

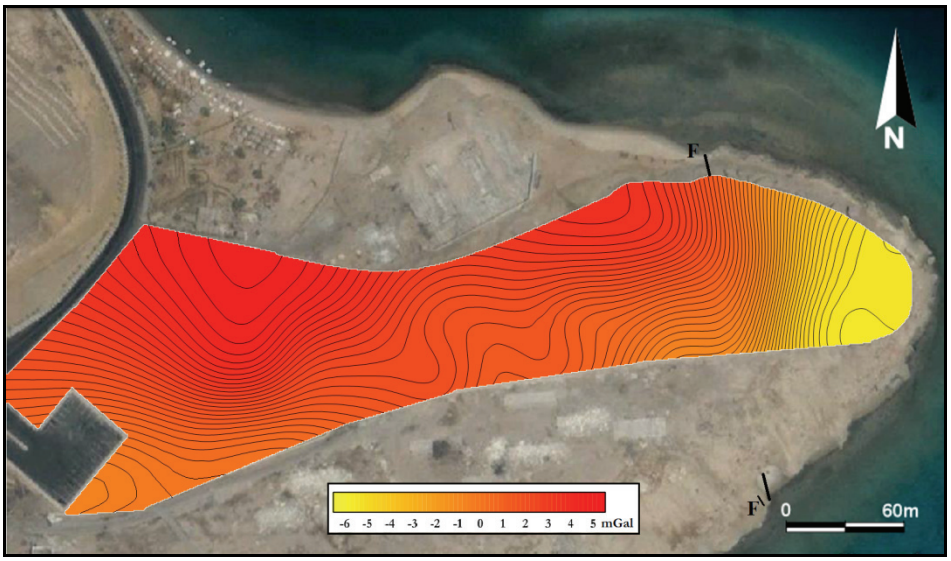

Fig. 8. Regional gravity anomaly map of the study area (Contour interval: 0.2mGal).

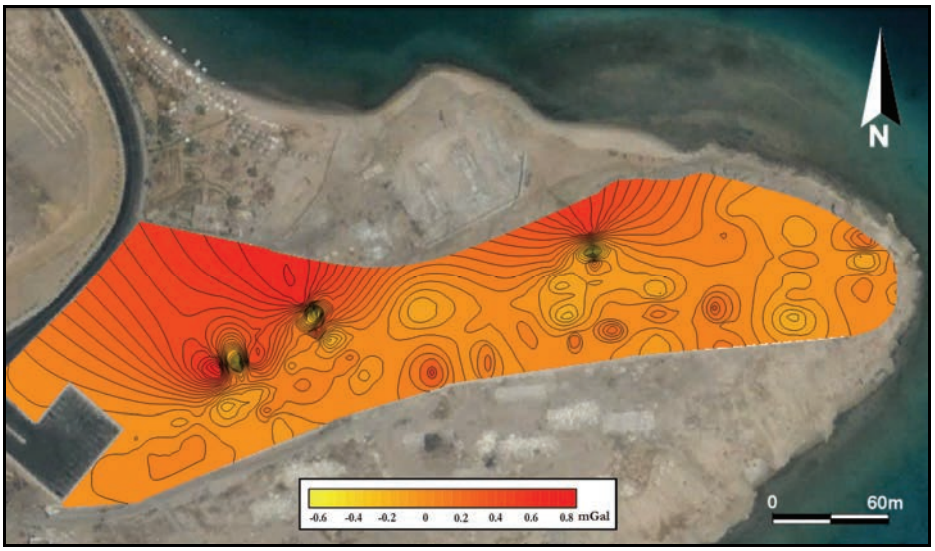

Fig. 9. Residual gravity anomaly map of the study area (Contour interval: 0.05 mGal).

The regional anomaly map clearly shows a north-south trending, steeply dipping fault F-F\ (Fig. 8). This fault was defined as an oblique slip fault, which has a dip slip component in which the down-faulted block plunged northward. A careful inspection of the location of the fault shows that it has a left-lateral strike slip component as well. The regional

gravity map also shows that the up-thrown block of the fault slightly tilts to the north direction.

The residual anomaly map clearly defines a number of local anomalies (Fig. 9), which are largely consistent with those depicted earlier by the magnetic survey. The two anomalies located at the western part of the residual gravity anomaly map coincide with the first and second anomalies on the magnetic maps. Both show four sets of semicircular closed contour lines. The contour line values of the central set decreases drastically inward, while the surrounding sets show inward increase in contour values. The shapes of these anomalies are correlated with that of a buried tank made of dense material and is empty or filled with low density material. The central part of the empty tank has certainly a very low density, whereas its walls are made of a high density material, such as reinforced concrete, which laterally changes to friable sedimentary rocks characterized by comparatively lower densities.

The third anomaly on the residual gravity map is located in the central part of the study area at about 137 meters to the northeast of the second anomaly. It corresponds to the third anomaly on the magnetic maps. This anomaly is characterized by its elliptical closed contour lines, which decrease in value towards the center. Its long axis is about 20 meters and trends in the northwest-southeast direction. It is surrounded from north and south by smaller circular anomalies that increase in value inwards. The shape of this anomaly and the perception of the nature of the buried structures in the study area may suggest the presence of yet another buried reinforced-concrete tank. The dimensions of this tank are similar to those of the first tank. The depth estimated from the residual gravity data is about 4.2 meters.

In the southwestern part of the study area, three small anomalies can be seen at about 20 meters to the south of the first and second anomalies. These three anomalies are characterized by elliptical closed contour lines, which increase in value towards their respective centers. The similarity in shape and the position of the anomalies on the residual gravity anomaly maps indicate that these anomalies refer to a buried pipeline extending to the south of the depicted tanks. The length of this pipeline is about 36 meters while its depth of burial is about 2.5 meters.

Another group of six similar anomalies are located parallel to the wall delimiting the southern border of the study area. These anomalies

are generally characterized on the residual gravity map by their elliptical closed contour lines, in which gravity values increase inward, which indicate the presence of high density objects. These six anomalies appear in all gravity profiles conducted perpendicular to the wall and at few meters away from it. The similarity in shape and the position of this set of anomalies very close to the wall, as shown in the residual gravity anomaly map (Fig. 9), are rather indicative of the presence of a long buried non-metallic pipeline and can be an extension of the previously depicted pipeline. The length of this pipeline is about 250 meters and its depth of burial is about 3 meters.

The gravity survey conducted on the study area revealed two different types of subsurface structures. They were distinguished into naturally occurring subsurface structures, or regional structures, and a group of artificial subsurface structures, or local structures. Regional structures in the study area are dominated by an oblique slip north-south trending fault located at the eastern part of the study area (Fig. 8). The impact of this fault on the spatial distribution of the polluting hydrocarbons in Sharm El-Maya Bay area is not quite clear. Local structures were divided into two main groups. The first group, which was also identified by the magnetic method, represents a number of buried storage tanks. They include three either empty or partially filled reinforced-concrete tanks. The second group represents a part of buried pipeline network that extends from near the first and second tanks and along the southern border of the study area.

Summary and Conclusion

A combined gravity and magnetic surveys were conducted on the Sharm El-Maya headland in order to investigate the source(s) of hydrocarbon contamination that devastated the Sharm El-Maya Bay more than a decade ago.

Field magnetic survey determined the locations of two main groups of buried oil-storage tanks. The first group included two adjacent reinforced-concrete tanks buried in the western section of the headland. The second group comprised two reinforced-concrete tanks with different characteristics. They are buried at the central and the eastern sections of the headland and are about 140 meters to the east of the first group.

These two tanks are similar in dimensions to those of the first group but they are buried at a greater depth of about 5 meters.

Gravity survey revealed two different types of subsurface structures, namely regional structures and local structures. Regional structures are dominated by an oblique-slip north-south-trending fault located at the eastern part of the study area. Local structures were subdivided into two main groups. The first group includes three reinforced-concrete tanks. These tanks are either empty or filled of a material of lower density such as hydrocarbons. The second group of local structures comprises two sub-parallel pipelines. These pipelines are possibly made of concrete, or asbestos, as they were not detected during the magnetic survey.

Integrating the abovementioned conclusions, which were based on the interpretation of geophysical data, the spatial distribution of total hydrocarbons, and other field observations, it is evident that there are three buried reinforced-concrete tanks and a buried pipeline beneath the headland (Fig. 10). These buried tanks may be empty or partially filled with hydrocarbons. These three tanks may represent the source of contamination occurred in the study area. These tanks still represent an imminent threat to Sharm El-Maya Bay area, in general, and to the northern beach of the headland and its fringing coral reefs, in particular.

Fig. 10. Locations of buried subsurface structures as inferred from the interpretation of the magnetic and gravity data (Red circles refer to buried tanks, dashed black line refers to fault, and the dashed white lines refer to buried pipelines).

Therefore, the study recommends that the buried tanks in the headland should be immediately excavated and evacuated from any stored oil products using appropriate techniques without bringing further damage to the environment. The three tanks should then be cleaned from any traces of petroleum products until an appropriate engineering solution is found to safely remove them from the area. A high-resolution geophysical survey tool, such as ground penetrating radar, can be used to survey depicted anomalous regions to precisely image the locations, depths, and dimensions of these tanks before the excavation process.

References

Allred, B., Fausey, N., Peters, L., Chen, , Daniels, J. and **Youn, H.** (2004) Detection of buried agricultural drainage pipe with geophysical methods. *Applied Engineering in Agriculture*, **32**: 307−318.

Butler, D. (1984) Microgravimetric and gravity gradient techniques for detection of subsurface cavities. *Geophysics*, **49**: 1084-1096.

Butler, D. (2001) Potential fields methods for location of unexploded ordnance. *The Leading Edge,* **20**: 890-895.

Cairo University (2001)*Report on Cleaning up Sharm El-Maya, Sharm El-Sheikh, southern Sinai, from the petroleum materials*. Center for Environmental Hazards Mitigation, Giza, Egypt.

Debeglia N. and **Dupont F.** (2002) Some critical factors for engineering and environmental microgravity investigations. *Journal of Applied Geophysics*, **50**: 435-454.

Dobrin, M. and **Savit, C.** (1988) *Introduction to Geophysical Prospecting*, Fourth Edition. McGraw-Hill Inc., New York, 867pp.

Furness, P. (2002) The magnetic fields of steel drums. *Journal of Applied Geophysics*, **51**: 63-74.

Gilkeson, R., Hiegold, P. and **Laymon, D.** (1986) Practical application of theoretical models to magnetometer surveys on hazardous waste disposal sites- A case history. *Ground Water Monitoring Review*, **6**: 54-61.

Griffin, W.R. (1949) Residual gravity in theory and practice. *Geophysics*, **14**: 39-56.

Hare, J., Ferguson, J., Aiken, C. and **Brady, J.** (1999) The 4-D microgravity method for waterflood surveillance: A model study for the Prudhoe Bay reservoir, Alaska: *Geophysics*, **64**: 78-87.

Hinze, W. (1990) The role of gravity and magnetic methods in engineering and environmental studies. In: Ward, *Geotechnical and Environmental Geophysics*, **1**: 75-126.

Horton, R. (2003) Application of magnetic and electromagnetic methods to locate buried metal. USGS Open-File Report 3-317.

Horton, R., Busby, J., Knoshaug, R. and **Powers, M.** (1993) Landfill mapping using multi-disciplinary geophysical techniques at the U.S. *Air Force Academy, Colorado Springs, CO. In: Proceedings of the Symposium on the Application of Geophysics to Engineering and Environmental Problems*, 109-128.

Khattab, R., Temraz, T., Kotb M. and **Hanafy, M.** (2006) Assessment of oil pollution in Sharm El-Maiya Bay, Sharm El-Sheikh, South Sinai, Egypt. *CATRINA, Egyptian Society For Environmental Sciences*, **1**: 33-40.

Marchetti, M., Cafarella, L., Di Mauro, D. and **Zirizzotti, A.** (2002) Ground magnetometric surveys and integrated geophysical methods for solid buried waste detection: a case study. *Annals of Geophysics*, **45**: 563-573.

Missiaen, T. and **Feller, P.** (2008) Very-high-resolution seismic and magnetic investigations of a chemical monition dumpsite in the Baltic Sea. *Journal of Applied Geophysics*, **65**: 142-154.

Mochales, T., Casas, A., Pueyo, E., Pueyo, O., Roman,T., Pocovi, A., Soriano, M. and **Anson, D.** (2008) Detection of underground cavities by combining gravity, magnetic and ground penetrating radar surveys: a case study from the Zaragoza area, NE Spain. *Environmental Geology,* **53**: 1067–1077.

Morsy, M., Soliman, F., Khattab, R., Rashed, M., and **El-Masry, N.** (2010) Implications of Environmental Monitoring of Oil Pollution in Sharm El-Maya Bay, Sharm El-Sheikh, Egypt. *CATRINA, Egyptian Society For Environmental Sciences*, **5**: 97-103.

NJDEP (2005) Field sampling procedures manual. New Jersey Department of Environmental Protection, 574 pp. <http://www.state.nj.us/ dep/srp/guidance/fspm/>.

Roberts, R., Hinze, W. and **Leap, D.** (1990) Application of the gravity method to the investigation of a landfill in glaciated midcontinent, U.S.A. *In: Ward, Geotechnical and Environmental Geophysics,* **2**: 253-259.

Rybakov, M., Goldshmidt, V., Fleischer, L. and **Rotstein, Y.** (2001) Cave detection and 4-D monitoring: A microgravity case history near the Dead Sea. *The Leading Edge*, **20**: 896-900.

Reynolds, J.M. (1997) *An Introduction to Applied and Environmental Geophysics*. John Wiley & Sons Ltd., Chichester, West Sussex, England, 796 pp.

Suez Canal University (1999) *Experts Committee Report to the High Appeal Court of Ismailia, Egypt*, Case No. 290/ 26.

Surfer (Version 8.00) "Surface Mapping Software" (1993-2002) Golden, 80401-1866 Colorado, USA: Golden Software, Inc.

Yule, D., Sharp, M. and **Butler, D.** (1998) Microgravity investigations of foundation conditions. *Geophysics*, **63**: 95-103.

مسح بطرق الجهد لتقصي مصدر التلوث في منطقة خليج شرم الميه بشرم الشيخ بمصر

مني مرسي، و محمد راشد[*]، و نبيل المصري[*]، و فاروق سليمان

قسم الجيولوجيا، كلية العلوم، جامعة قناة السويس، الإسماعيلية – مصر

[*] كلية علوم الأرض، جامعة الملك عبدالعزيز، جدة – المملكة العربية السعودية

المستخلص. يمثل تلوث مياه خليج شرم الميه تهديدًا خطيرًا للحركة السياحية المزدهرة التي تشهدها منطقة شرم الشيخ. وقد أثبتت التحاليل الكيميائية التي تم أخذها من مياه الخليج ومن رواسب قاع الخليج وكذلك عينات التربة من المنطقة المحيطة بالخليج وجود مستويات مرتفعة من التلوث بهذه العينات. وبناء عليه فقد تم إجراء مسح جيوفيزيائي باستخدام طريقتي المغنطيسية والتثاقلية لتحديد مصدر هذا التلوث وقد دللت نتائج المسح المغنطيسية علي وجود أربعة مواقع محتملة لخزانات صناعية مدفونة في المنطقة. وقد أكد المسح التثاقلي وجود ثلاثة من الخزانات التي كشفها المسح المغنطيسي وكذلك كشف المسح التثاقلي عن وجود فالق ضخم يقطع شرق منطقة الدراسة من الشمال إلى الجنوب. هذا وتوصي هذه الدراسة بمسح المناطق التي تم تحديدها عن طريق المسح المغنطيسية والتثاقلي بأحد الطرق الجيوفيزيائية الإضافية التي توفر صورًا عالية الجودة مثل طريقة المسح الراداري الأرضي وذلك لتوضيح توزيع وأشكال وأبعاد الخزانات التي تم اكتشافها.